Electrically Tunable All-Dielectric Metasurfaces Integrated With Nematic Liquid Crystals for Information Encryption

Chuan Shen, Jiali Sun , Yifei Qi, Shiqi Lv, and Sui Wei

Abstract—As artificially designed two-dimensional (2D) arrays of subwavelength nanostructures, metasurfaces provide a new avenue for the design of static planar optics. However, one would prefer a dynamic modulation of the metasurface in the event of practical applications. As a potentially important technique for information security, meta-holographic encryption has the characteristics of subwavelength pixels, precise control, and high safety factor. In this paper, by integrating birefringent liquid crystals (LCs) with all-dielectric metasurfaces in combination with visual cryptography (VC), we demonstrate a tunable metasurface with an information encryption function in the visible range. In the encryption process, the secret image is hidden in a set of unidentifiable and orthogonal arranged phase-only meta-holograms with high security of concealment. In the decryption process, the generated meta-hologram is illuminated by a plane wave and an electric field across the LC layer is applied to superimpose the reconstructed holographic patterns, thus we could acquire the secret image. Therefore, the decryption method can be flexibly and sufficiently adjusted with applied field under monitorable condition. For this reason, it is useful in enhancing the diversity of information hiding methods and improving the security of information. Our method can be extended to other similar applications.

Index Terms—Metasurfaces, electrically tunable, liquid crystals, information encryption.

I. INTRODUCTION

METASURFACES are 2D nanostructures consisting of metal or dielectric materials that offer a powerful tool to achieve light modulation of amplitude, phase, and polarization [1]–[3]. With the development of nanotechnology and the maturity of the fabrication process, it is possible to fabricate structures with individual feature sizes much smaller than the size of a wavelength of the light, which means that even if the structural elements are discrete, the manipulation of wavefronts can be regarded as identical with the case of a continuous one [4]. Consequently, metasurfaces provide potential feasibility for a plethora of applications such as holographic display [5], [6], beam shaping [7], [8], data storage [9], encryption and anti-counterfeiting [10], color printing [11], and optical communication [12], [13]. Compared with metasurfaces composed of metal nanoantennas with great ohmic loss, all-dielectric metasurfaces have attracted tremendous attention due to their high efficiency and complementary metal oxide semiconductor-compatible manufacturing process, which has great potential for practical applications. To date, most metasurface systems are based on static designs where their optical properties are fixed during the fabrication process. However, the manipulation mechanism of metasurfaces is based on the horizontal dimensions of the antennas rather than longitudinal thickness, makes them be a flat and ultra-thin component, and can be easily integrated together with other components. Many novel optical tunable metasurfaces that operate by means of phase-change materials [14], free-carrier effects [15], mechanical drive [16], chemical reactions [17], and manipulation of the surrounding environment [18], have been explored in recent years. Among them, the liquid crystal (LC) device is one of the most important and promising devices in practice, relying on the well-established expertise from the LC display industry [19]. Specifically, the effective optical birefringence of the LCs depends on their internal structure and allows the orientation of the LC molecules to be changed by means of an external electric field. As the voltage gradually changes, the nematic LCs (NLCs) platform is available to control the polarization state of the outgoing light [20]. Thus, the combination of LCs and metasurfaces can provide additional design ideas for active light modulation applications [21].

Information security technology is gaining more and more attention in today's rapidly developing society. With its excellent stability, long durability, as well as high resolution, and high data density, the metasurfaces are ideal for information hiding encryption. Zhao et al. implemented the rod slot antennas and C-shaped slot antennas are used as building blocks to achieve multi-image hiding and seeking with polarization control in the terahertz band in 2019 [22]. Li et al. hided the encrypted images in two metasurfaces respectively, and superimposed the

Chuan Shen is with the Key Laboratory of Intelligent Computing & Signal Processing, Ministry of Education, Anhui University, Hefei 230601, China, and also with the Key Laboratory of Modern Imaging and Display Technology of Anhui Province, Anhui University, Hefei 230601, China (e-mail: shenchuan@ahu.edu.cn).

Jiali Sun, Yifei Qi, Shiqi Lv, and Sui Wei are with the Key Laboratory of Intelligent Computing & Signal Processing, Ministry of Education, Anhui University, Hefei 230601, China (e-mail: 1020251670@qq.com; 785475034@qq.com; 570943558@qq.com; swei@ahu.edu.cn).
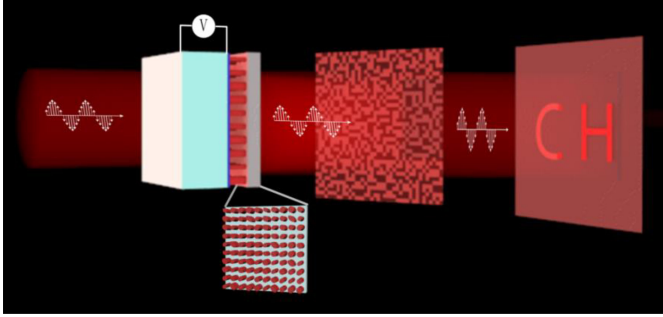
Fig. 1. Schematics of the principle and structure of electrically tunable all-dielectric metasurface. When the applied liquid crystal voltage is incorrect, meta-holographic encryption image cannot be obtained and vice versa. For the sake of intuitive explanation, two images are separated in diagram for these two cases, but in reality, they are in the same plane.
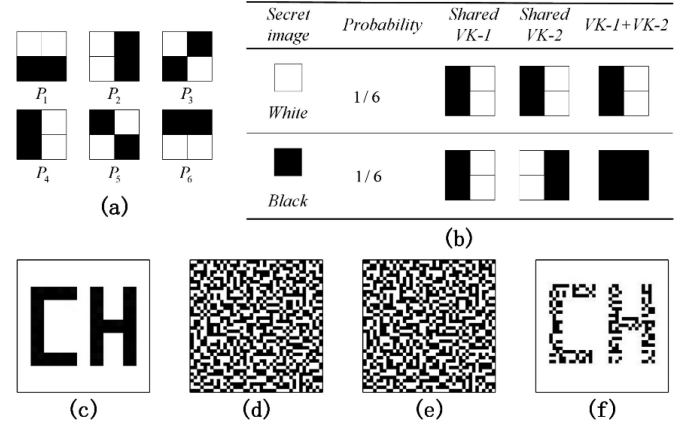

Fig. 2. VC encryption principle: (a) Six possible expansion; (b) An example of the encoding process for a white and black pixel of the secret image; (c) Target image; (d)-(e) Shared image1 and image2; (f) Recovered image.

reconstructed holograms by optical method to realize the reproduction of the target image [23]. Both of the methods use static metasurfaces for achieving hidden encryption of information, thus we would like to extend metasurfaces to a tunable one for information encryption and hiding, which can enhance the diversity of information hiding methods and greatly enhance the security level of information [24].

In this paper, we integrate all-dielectric metasurface with birefringent NLCs to achieve dynamic tunability for optical information encryption. According to visual cryptography (VC), the target image is hidden into a group of shared images by pixel expansion encoding, and the holographic phase encoding technology is used to map the group of images onto the polarization-sensitive dielectric metasurface, combined with the real-time tunable birefringent LC to realize the hiding and reproduction of encrypted images.

II. DESIGN AND METHOD

The schematic of our approach to implement the dynamically tunable polarization-sensitive holographic interface is shown in Fig. 1. We integrate all-dielectric metasurface with a birefringent LC layer, where the metasurface composed of titanium dioxide (TiO$_2$) elliptical nanopillars with different radius parameters arranged periodically. This method provides better excitation of LC performance and higher device efficiency than wrapping nanoantennas directly in LCs, and also provides a simpler device preparation process. When no voltage is applied across the LC cell, there is no molecular rotation and no useful information can be obtained. When the correct voltage is applied, the deflection direction of the LC molecule changes, thus changing the polarization state of the incident light and allowing the reconstruction of the hidden "CH" hologram in the far field.

The technique of VC is an important component of information security that enables encryption of image information, and can be simply divided into two operations [25]. The first step is secret sharing, which generates a set of shared images, and the second step is secret recovery, which makes people observe different visual effects by different light penetration rates of black and white pixel points, so as to achieve the purpose of

recovering secret images. Fig. 2 illustrates the image encryption design method. A binary secret image is generated as multiple shared images containing noise by dividing each secret pixel point into a pixel block consisting of 2×2 sub-pixels. As shown in Fig. 2(a) and (b), each black and white pixel point in the binary image has six equal possibilities to choose from. The white pixel points are randomly diffused into identical shared pixel blocks, and the black pixel points are randomly diffused into complementary shared pixel blocks. Since the diffusion scheme of each pixel is random, as shown in Fig. 2(c)–(f), the encrypted image is independently converted into two uncorrelated mosaic-like gray-scale distributions, and the secret image is obtained when the shared images are aligned and superimposed with each other. In our method, it is necessary to convert the binarized shared image into the phase-only hologram to further enhance security. Note that, for getting high-quality phase-only holograms, two shared images could be made equal to each other by the same ratio with magnification and then be iterated by the optimized Gerchberg-Saxton (GS) algorithm to generate the corresponding holograms [26].

III. SIMULATIONS OF TUNABLE METASURFACE

In our design, the unit cell of the metasurface is designed as TiO$_2$ elliptical nanopillars structure with anisotropic properties due to the highly refractive nature. Fig. 3(a) illustrates a single nanopillar positioned on a glass substrate, each elliptical nanopillar is regarded as a waveguide truncated on both sides and operates as a low-quality factor Fabry-Perot resonator. The elliptical cross-section of the waveguide leads to waveguide modes polarized along the two elliptical radii R_x and R_y with different effective refractive indices, so that each elliptical cylinder exerts a polarization-dependent phase shift on the transmitted light [27]. For dielectric metasurfaces, the effect of the change in resonant frequency on the phase of the transmitted light is greater than on the amplitude in a certain frequency range, and hence it can be roughly assumed that the amplitude values of the transmitted light propagating along the radii R_x and R_y of the elliptical nanopillars are equal and only the phase is
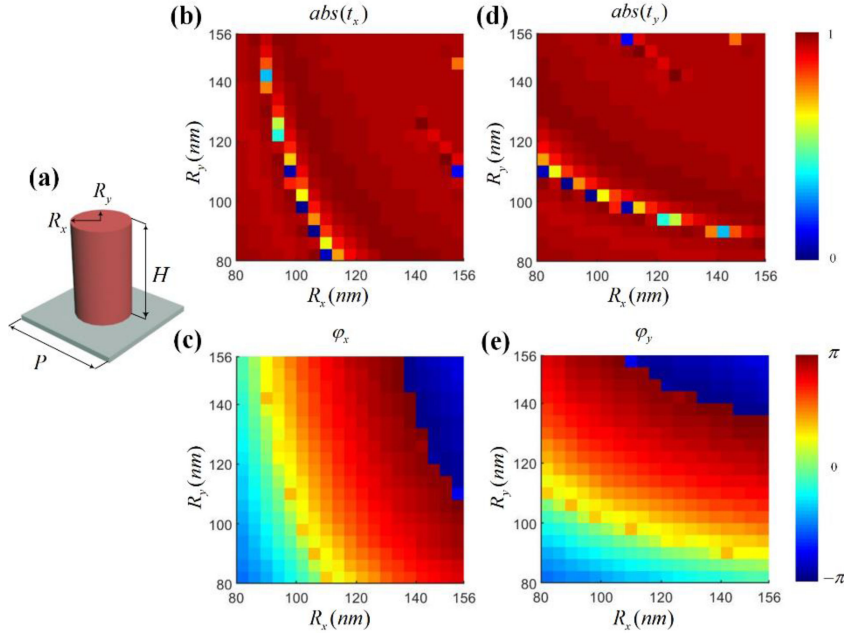
Fig. 3. Simulated amplitude and phase of the transmission coefficients refer to our designed TiO$_2$ nanopillars. (a)Schematic of a TiO$_2$ nanopillar positioned on a glass substrate. (b)-(e) Simulation results for the amplitude and phase of the unit cell shown for a 2D parameter optimization. Radii R_x and R_y of the elliptical nanostructure are both swept in the range of 80-156 nm at an incident wavelength of 671 nm.

changed. Thanks to the high refractive index characteristic of the dielectric material, mode fields can be effectively localized within the unit cell, so coupling between adjacent structures is usually negligible and each elliptical nanopillar cell can be considered as a pixel unit [28].

The structure is operated at a wavelength of 671 nm and the parameters of the unit cell are optimized by a commercial soft tool (FDTD solutions, Lumerical) based on the Finite-Difference Time-Domain (FDTD) method. The height H of the TiO$_2$ elliptical nanopillars is 650 nm, arranged in a square unit lattice with a period P of 500 nm. Due to the symmetry, the normally incident light linearly polarized along one of the elliptical radii acquires only phase as it passes through the array, with the phase shift applied by the array to the x and y-polarized light (i.e., φ_x and φ_y) varying with the radii parameter of the ellipse. As shown Fig. 3, the radii R_x and R_y of the elliptical nanopillars were swept in the range of 80 nm to 156 nm, and any combination of R_x and R_y can be obtained simultaneously by proper selection of radii R_x and R_y from the sweep above, with the corresponding intensity transmission coefficients (i.e., $abs(t_x)$ and $abs(t_y)$). In our design, six proper radii (80, 91, 99, 110, 128 and 156nm) were chosen in each polarization channel to ensure that the phase shift of either φ_x or φ_y can cover the entire 0-2π range while we skip some points with low efficiency exist in transmission maps in order to maintain a uniform amplitude distribution with high efficiency. As a result, the high performance of the platform can be achieved. The phase information of two uncorrelated holograms was discrete designed and mapped onto the metasurface based on the obtained elliptical radii parameters.

In order to achieve the tunability of the active metasurface and realize electric-field-responsive meta-holograms. The

commonly used negative dielectric anisotropy MBBA LC material for our selection, a widely used NLC for displays, whose refractive index change between the voltage on and voltage off states is about 0.24. In the simulations, to avoid unnecessary phase shifts caused by the near-field interaction between the LC layer and the metasurface, the NLC is designed to be layered with the metasurface when using FDTD simulations [29]. Among them, the length and width of the LC layer are the same as the size of the integrated metasurface underneath. The rearrangement of the LC molecules changes the effective refractive index in the LC cell, thereby exhibiting different optical properties from the original state, when the orientation of the LC molecules and the polarization of the incident beam from outside the NLC can be controlled by an external electric field.

To illustrate the optical properties of our structure, as shown in Fig. 4, the light incident on the structure is linearly polarized at 45° relative to the x-y-plane in the two respective cases with no voltage applied and voltage applied. Note that, radii R_x and R_y of the elliptical nanopillar cells are also placed at 45° corresponding to the x-y-plane, respectively.

In the first case, LC molecules have strong anchoring force on the adjacent surface and remain aligned perpendicular to the surface, corresponding to $n_x = n_o$, $n_y = n_o$, $n_z = n_e$, where n_o and n_e are the refractive indices along the ordinary and extraordinary axes. At this time, NLC does not produce birefringence effect, there is no polarization state change, thus only one of the shared images in the far field is generated and the encrypted image cannot be acquired.

While in the case of the correct voltage applied, the direction of the LC molecules will gradually be perpendicular to the direction of the electric field and parallel to the y-axis as the applied electric field changes, corresponding to $n_x = n_o$,
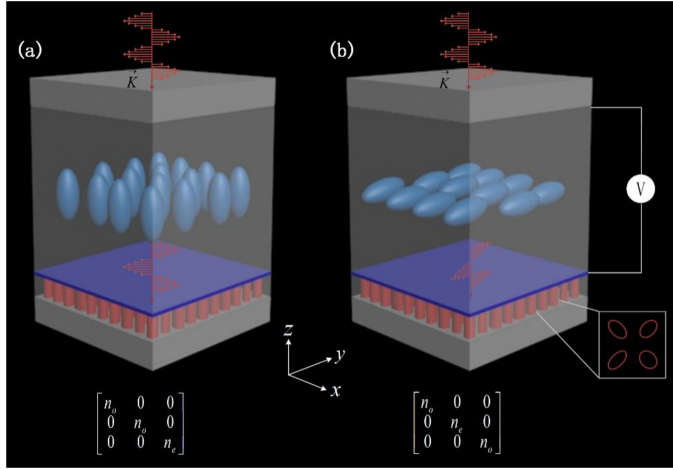
Fig. 4.   Schematic of the liquid-crystal-integrated metasurfaces. (a)Under no voltage state, the initial LC director in the vertical orientation (homeotropic alignment), and the polarization state of the outgoing light is not changed at this time. (b) When the voltage is correct applied, the LC directions parallel to the y-axis (planar alignment) and change the polarization state of the incident light.
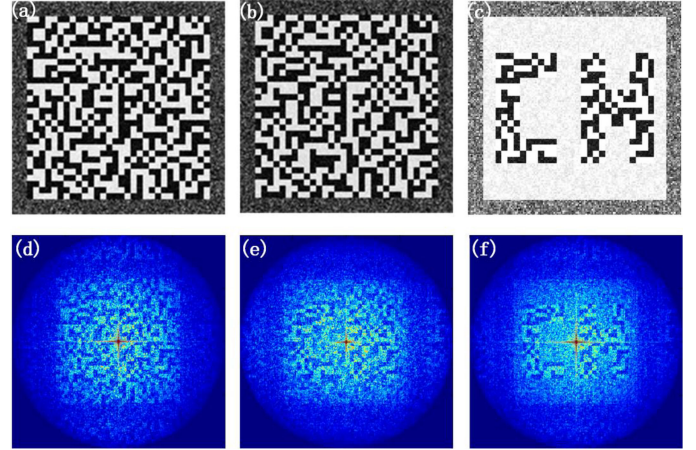

Fig. 5.   Simulation Results. (a)-(c) are the set of shared images and target image recovered by the improved GS algorithm. (d) one of the shared images obtained by the metasurface simulation. (e) Far-field reconstruction image simulated by metasurface when the incorrect voltage is applied. (f) the target image "CH" reconstructed from the metasurfaces.

$n_y = n_e$, $n_z = n_o$. The polarization plane of the incident light is in the same plane as the director of the LC molecules, and the incident light can be decomposed into two components parallel and perpendicular to the long axis of the LC molecules. Due to the different light propagation speeds, the polarization state of the outgoing light changes. At this time, a group of shared images corresponding to metasurface holograms are superimposed at the same position in the far field to obtain the encrypted image.

IV. RESULTS AND DISCUSSIONS

Simulation experiments based on the FDTD method are performed to demonstrate our method. Consider a uniform anisotropic medium at a wavelength of 671 nm, $n_e = 1.78$ and $n_o = 1.54$, an operating temperature of 20 °C. Due to the ultra-thin thickness of the ITO electrode layer, we ignored it in the simulation. In considering homogeneous NLCs of both configurations, we neglected the possible effects due to the stable anchoring of the LC molecules to the nanostructure, a phenomenon that reduces the LC anisotropy. We also assumed the rotation of the LC molecules to an ideal state, and the distance between the NLC and the metasurface is relatively close.

Taking into account the limitations of our computer performance, the NLC thickness is designed to be 0.7 μm, and shared images of 140×140 pixels are encoded for simulation. Holographic images are reconstructed by Fourier transform to recover the invisible phase-only holograms as binary shared images, where the polarization state will be deflected after the incident beam passes through the LC layer, so a set of shared images with orthogonal polarization can be reconstructed and superimposed at the same location. Thus, the extracted secret information can be received directly by the human visual system without any other decryption calculation.

Fig. 5(a)–(c) illustrate two shared images and target image recovered by the optimized GS algorithm. Note that, we use a zero-padding method to deal with the complex amplitude before iteration. The holographic images obtained by the metasurface simulation are rebuilt by Fourier transform at a distance of 1m as shown in Fig. 5(d)–(e), respectively. When no voltage is applied, there is no change in the polarization state of the incident light, and thus only one of shared holographic images is obtained in the far field (Fig. 5(d)). And when the incorrect voltage is applied, there is a mosaic-like reconstructed image in the far field, and the encrypted image cannot be obtained at this time (Fig. 5(e)) as the LC molecules are not all deflected to be parallel to the electric field direction. Two shared images with orthogonal polarization can be superimposed at the same position through the deflection of LC molecules with correct voltage applied. Although there are some random noises like speckle noises on the images due to the phase dispersion, it is still possible to achieve the reproduction of hidden image "CH" in Fig. 5(f). The contrast of the reproduced secret image is still high enough to be clearly identified without any lenses or other optical components. There are many attractive properties of holography as a potential information encryption technique. The advantages include a better safety and reliability can be attributed to a certain redundancy of the hologram. Because a defect that obscures or destroys a very localized area on the hologram will not create a localized defect in the reconstruction image. A second advantage, associated particularly with the electrical properties of LCs. While there is a change in the LC voltage, that is to say, it can be judged that the encrypted information may have been obtained, and tunable metasurfaces can further improve the security of encryption according to the anti-monitoring strategy. In practice, the thickness of the NLC layer can be designed as a basic specification parameter of the display device. (e.g. 5 μm). In classical holography, if the optical system is to produce high-quality holographic image, then one could fabricate the hologram consists of numerous

pixels manufactured by mature processing techniques (such as lithography and nanoimprinting). For metasurface holography, in the same, the larger the number of pixels, the higher the image resolution. However, greater amounts of subwavelength pixels also result in higher data process and fabricating costs, this proves to be a difficult task [30].

V. CONCLUSION

In summary, we have achieved holographic optical reproduction of encrypted information using an electrically tunable metasurface. The VC method can convert a secret image into a set of binarized shared images, and phase-only holograms can be obtained using the optimized GS algorithm. We employ TiO$_2$ dielectric material with a high refractive index to design the unit cell, which can achieve full phase coverage with high transmittance, and its subwavelength structure is easy to hide and not easily damaged or forged. A set of phase-only holograms are mapped onto the metasurface, and the NLC that realizes the direction deflection of the LC molecules by applying an external electric field is placed on the upper layer of the metasurface, which can realize real-time and fast adjustment without affecting the performance of the metasurface. The active tunable metasurface can provide a powerful, efficient, and lightweight new platform for optical information encoding, encryption, anticounterfeiting, and concealment technologies.

REFERENCES

[1] C. L. Holloway, E. F. Kuester, J. A. Gordon, J. O'Hara, J. Booth, and D. R. Smith, "An overview of the theory and applications of metasurfaces: The two-dimensional equivalents of metamaterials," *IEEE Antennas Propag. Mag.*, vol. 54, no. 2, pp. 10–35, Apr. 2012.

[2] N. Yu and F. Capasso, "Flat optics with designer metasurfaces," *Nature Mater.*, vol. 13, no. 2, pp. 139–150, 2014.

[3] X. Lou, M. Pu, X. Ma, and X. Li, "Taming the electromagnetic boundaries via metasurfaces: From theory and fabrication to functional devices," *Int. J. Antennas Propag.*, vol. 2015, 2015.

[4] J. Guo *et al.*, "Polarization multiplexing for double images display," *Opto-Electron. Adv.*, vol. 2, no. 7, 2019, Art. no. 180029.

[5] P. Genevet and F. Capasso, "Holographic optical metasurfaces: A review of current progress," *Rep. Prog. Phys.*, vol. 78, no. 2, 2015, Art. no. 024401.

[6] J. P. B. Mueller, N. A. Rubin, R. C. Devlin, B. Groever, and F. Capasso, "Metasurface polarization optics: Independent phase control of arbitrary orthogonal states of polarization," *Phys. Rev. Lett.*, vol. 118, no. 11, 2017, Art. no. 113901.

[7] S. Sun *et al.*, "High-efficiency broadband anomalous reflection by gradient meta-surfaces," *Nano Lett.*, vol. 12, no. 12, pp. 6223–6229, 2012.

[8] T. Li *et al.*, "Generation and conversion dynamics of dual bessel beams with a photonic spin-dependent dielectric metasurface," *Phys. Rev. Appl.*, vol. 15, no. 1, 2021, Art. no. 014059.

[9] R. Zhao *et al.*, "Multichannel vectorial holographic display and encryption," *Light: Sci. Appl.*, vol. 7, no. 1, 2018, Art. no. 95.

[10] J. Deng *et al.*, "Multiplexed anticounterfeiting meta-image displays with single-sized nanostructures," *Nano Lett.*, vol. 20, no. 3, pp. 1830–1838, 2020.

[11] Y. Nagasaki, M. Suzuki, and J. Takahara, "All-dielectric dual-color pixel with subwavelength resolution," *Nano Lett.*, vol. 17, no. 12, pp. 7500–7506, 2017.

[12] J. Wang *et al.*, "Terabit free-space data transmission employing orbital angular momentum multiplexing," *Nature Photon.*, vol. 6, no. 7, pp. 488–496, 2012.

[13] S. Li *et al.*, "Multidimensional manipulation of photonic spin hall effect with a single-layer dielectric metasurface," *Adv. Opt. Mater.*, vol. 7, no. 5, 2019, Art. no. 1801365.

[14] S. Y. Lee *et al.*, "Holographic image generation with a thin-film resonance caused by chalcogenide phase-change material," *Sci. Rep.*, vol. 7, no. 1, 2017, Art. no. 41152.

[15] T. Lewi, P. P. Iyer, N. A. Butakov, A. A. Mikhailovsky, and J. A. Schuller, "Widely tunable infrared antennas using free carrier refraction," *Nano Lett.*, vol. 15, no. 12, pp. 8188–8193, 2015.

[16] S. C. Malek, H. S. Ee, and R. Agarwal, "Strain multiplexed metasurface holograms on a stretchable substrate," *Nano Lett.*, vol. 17, no. 6, pp. 3641–3645, 2017.

[17] M. Matuschek *et al.*, "Chiral plasmonic hydrogen sensors," *Small*, vol. 14, no. 7, pp. 1702990, 2018.

[18] J. Li, Y. Chen, Y. Hu, H. Duan, and N. Liu, "Magnesium-based metasurfaces for dual-function switching between dynamic holography and dynamic color display," *ACS Nano*, vol. 14, no. 7, pp. 7892–7898, 2020.

[19] Y. Hu *et al.*, "Electrically tunable multifunctional polarization-dependent metasurfaces integrated with liquid crystals in the visible region," *Nano Lett.*, vol. 21, no. 11, pp. 4554–4562, 2021.

[20] C. Williams *et al.*, "Engineered pixels using active plasmonic holograms with liquid crystals," *Physica Status Solidi (RRL)-Rapid Res. Lett.*, vol. 9, no. 2, pp. 125–129, 2015.

[21] A. Lininger *et al.*, "Optical properties of metasurfaces infiltrated with liquid crystals," *Proc. Nat. Acad. Sci.*, vol. 117, no. 34, pp. 20390–20396, 2020.

[22] H. Zhao, C. Zhang, J. Guo, S. Liu, X. Chen, and Y. Zhang, "Metasurface hologram for multi-image hiding and seeking," *Phys. Rev. Appl.*, vol. 12, no. 5, p. 054011, 2019.

[23] Z. Li *et al.*, "Efficient dielectric metasurface hologram for visual-cryptographic image hiding," *Opt. Exp.*, vol. 27, no. 14, pp. 19212–19217, 2019.

[24] Z. Deng, Q. Tu, and X. Li, "Multi-dimensional metasurface and its application in information encryption and anti-counterfeiting," *Infrared Laser Eng.*, vol. 49, no. 9, pp. 20201034–1–20201034–16, 2020.

[25] H. Yamamoto, Y. Hayasaki, and N. Nishida, "Securing information display by use of visual cryptography," *Opt. Lett.*, vol. 28, no. 17, pp. 1564–1566, 2003.

[26] L. Chen, H. Zhang, Z. He, X. Wang, L. Cao, and G. Jin, "Weighted constraint iterative algorithm for phase hologram generation," *Appl. Sci.*, vol. 10, no. 10, 2020, Art. no. 3652.

[27] A. Arbabi, Y. Horie, M. Bagheri, and A. Faraon, "Dielectric metasurfaces for complete control of phase and polarization with subwavelength spatial resolution and high transmission," *Nature Nanotechnol.*, vol. 10, no. 11, pp. 937–943, 2015.

[28] A. Arbabi, Y. Horie, A. J. Ball, M. Bagheri, and A. Faraon, "Subwavelength-thick lenses with high numerical apertures and large efficiency based on high-contrast transmitarrays," *Nature Commun.*, vol. 6, no. 1, 2015, Art. no. 7069.

[29] I. Kim *et al.*, "Stimuli-responsive dynamic metaholographic displays with designer liquid crystal modulators," *Adv. Mater.*, vol. 32, no. 50, 2020, Art. no. 2004664.

[30] Q. Jiang, L. Cao, H. Zhang, and G. Jin, "Improve the quality of holographic image with complex-amplitude metasurface," *Opt. Exp.*, vol. 27, no. 23, pp. 33700–33708, 2019.